J. Eur. Opt. Society-Rapid Publ. 2024, **20**, 1

https://doi.org/10.1051/jeos/2023047
Available online at: https://jeos.edpsciences.org

Journal of the European Optical Society-Rapid Publications

RESEARCH ARTICLE

OPEN ACCESS

Detection of zinc in pig feed based on the cavities of different shapes combined with LIBS

Jing Li[1,2], Mengqin Huang[1], Shujia Wu[1], Zihao Liu[1], Mingyin Yao[1,2], Muhua Liu[1,2], and Long Xue[1,2,*]

[1] College of Engineering, Jiangxi Agricultural University, Nanchang 330045, China
[2] Jiangxi Key Laboratory of Modern Agricultural Equipment, Nanchang 330045, China

Received 8 November 2023 / Accepted 18 December 2023

Abstract. Considering the serious risks posed by the heavy metals present in pig diets, monitoring and controlling the amount of these metals is crucial. The laser-induced breakdown spectroscopy (LIBS) is a promising technique for performing elemental analysis due to its unique advantages, such as rapid, in situ, nondestructive, and online detection of various minerals. In order to improve the detection accuracy and detection limit (LOD) of elements, the spatial constraint combined with laser-induced breakdown spectroscopy (CC-LIBS) is used to detect the quantity of zinc in pig feed and achieve the detection of samples with lower concentrations. Zn I 480.86 nm is selected as the characteristic spectral line, and the effects of different two-dimensional (cylindrical) and three-dimensional (hemispherical, truncated cone) cavities on the enhancement factor are compared under different time delays. The results show that the optimal conditions include a truncated cone cavity D5H3, a delay time of 2.08, and an enhancement factor of 3.01 associated with the analytical spectral line. The detection limit of zinc in samples under CC-LIBS is 62.67 mg/kg (the recommended quantity of zinc in pig diet mentioned in the safe use of feed additives is 43–80 mg/kg), which is 35.65% lower than that under the LIBS (97.39 mg/kg). Therefore, this work provides a new test basis and idea for the detection of zinc in pig feed.

Keywords: Spatial constraint, Laser induced breakdown spectroscopy, Pig feed, Zinc, Detection limit.

1 Introduction

Zinc is an essential nutrient for the health and growth of pigs [1, 2]. Unlike most of the other minerals except copper, zinc is a unique nutrient as it provides an antibacterial effect, and effectively reduces the incidence and severity of diarrhea in pigs after weaning. Zinc is added to the weaned piglet diet at pharmacological levels (2000–3000 mg/kg) for promoting growth [3]. However, due to a small amount of zinc already present in the bodies of pigs, more than 90% of zinc is excreted in feces for subsequent application to farmlands [4, 5]. The previous studies presented in literature have shown that using manure in agricultural soils for meeting the requirements of nitrogen and phosphorus removal rates leads to the accumulation of excessive zinc in soil, resulting in ecological toxicity [6]. In addition, the excessive zinc in the diet of pigs also affects the development of antibiotic and antibiotic activity [7]. Recently, new regulations have been implemented in China, with a maximum limit of zinc in piglets (≤25 kg) compound feed set at 110 mg/kg. These regulations also state that the use of zinc oxide or basic zinc chloride up to 1600 mg/kg is allowed on this basis during the first two weeks after weaning [8]. Therefore, monitoring and controlling the zinc levels during the production of pig feed are essential to ensure that excessive amounts of zinc do not reach the consumers.

The well-known methods for detecting the amount of zinc in pig feed include atomic absorption spectrometry (AAS) [9], spectrophotometric (SP) [10], and inductively coupled plasma mass spectrometry (ICP-MS) [11], etc. However, the detection processes adopted in these methods are complex, time-consuming, and require the introduction of a large number of chemical reagents, which may become the cause of environmental pollution. As a result, it is not possible to perform real-time analysis of pig diet. As compared with the aforementioned methods, the LIBS does not require complicated sample pretreatment, is not time-consuming, and achieves simultaneous detection of multiple elements [12]. However, the detection sensitivity of this technique is low, detection limit is high, and its application in the detection of trace elements is limited. The researchers have developed various methods for enhancing the LIBS signal, such as double-pulse LIBS [13], spark discharge assisted LIBS [14], nanoparticles LIBS [15], microwave-assisted LIBS [16], and magnetic field confinement LIBS

* Corresponding author: ultimata@163.com

[17]. Although these methods are successful in performing elemental analysis, they also increase the complexity of LIBS systems. In recent years, many studies have shown that the spatial confinement LIBS has unique advantages. This method only requires minor changes in the original LIBS system and a simplest device, resulting in the lowest cost. Additionally, it enhances the signal repeatability and improves the plasma morphological stability [18].

Therefore, the spatial confinement LIBS-based method is widely used in applications. The constraints include parallel plate constraint [19] or flat mirror constraint [20], cylindrical constraint [21], and conical constraint [22] or hemispherical constraint [23]. The spatial constraints on the plasma range from one dimension to two dimensions to three dimensions, with higher dimensional constraint resulting in more enhancement. The spatial confinement effect of plasma is based on the accompanying shock wave. Furthermore, the evolution distance of the shock wave is influenced by the linear distance from the center of the plasma plume to the wall of the spatial confinement chamber. The longer this distance is, the weaker is the evolving shockwave. This reduces the compression of the plasma and lowers the enhancement effect. On the contrary, if this distance is short, the shock wave rebounds quickly, thus enhancing the short-lived continuous and ion spectrums, which is not good for performing elemental analysis using LIBS. However, the effect of CC-LIBS on the enhancement and stabilization of plasma emission intensity depends not only on the size of the cavity, but also on the delay caused during acquisition, which is a key parameter [24]. The enhancement of the plasma emission spectrum and the stability of the plasma core only exist within a certain time window. Therefore, it is necessary to study the delay time parameters.

Meng et al. studied the combination of LIBS, flat mirror, and temperature control enhancement methods. The results showed that the enhancement factors of Cd, Fe, Al, and Pb in soil were 2.50, 2.78, 2.66, and 2.47, respectively [25]. Based on the time evolution of LIBS constrained by a cylindrical cavity and the action of nanoparticles, Ren et al. observed that when the acquisition delay time is 1μs, the plasma generated by the alloy sample exhibits the highest enhancement factor under the dual action. Ni II 221.65 nm and C I 193.09 nm spectral lines were selected for performing analysis, and the enhancement factor reached 2.1 [26]. Xu et al. used conical cavity LIBS to study the spectral lines of Cu I 5153.2 nm and Cu I 521.82 nm. The results show that the spectral intensities of two lines were enhanced 2–3 times [22]. To the best of our knowledge, the application of LIBS technology for performing analysis of zinc content in pig feed has not been reported. Moreover, there are only few researchers that have compared the shape of these three cavities.

In this work, CC-LIBS is used to study the spectral intensity enhancement factor of zinc in pig feed. The proposed method compares two-dimensional (cylindrical) and three dimensional (hemispherical and truncated cone) spatial confinement cavities of different sizes. The analysis based on optimal spatial confinement cavity and delay time shows that the CC-LIBS improves the quantitative accuracy. At the same time, the detection limit of elements is also reduced to satisfy the allowed national standard range.

2 Materials and methods

2.1 Experimental setup

The experimental setup is presented in Figure 1. It mainly consists of a water cooling system, Q-switched nanosecond Nd:YAG coaxial dual-beam pulsed laser with wavelength of 1064 nm; pulse width of 6–8 ns and a frequency of 2 Hz (Vlite-200, Beamtech Ophtronics Co, Ltd, China), two-channel spectrometer (AvaSpec-ULS2048-2-USB2, Avantes, Netherlands) having a band range of 206.28–331.41 nm and 321.46–481.77 nm with 2048 data points in each channel, optical fiber probes, optical fiber, reflector (45° reflector and perforated reflector), focusing lens and two-dimensional rotating platform that rotates clockwise at a uniform speed (SC300 controller, Beijing Zolix Instruments Co., LTD.). Shenyang automatic delay device is used to control the delay interval of laser pulse and spectrometer acquisition, and the time interval of double pulse.

The spatial confinement cavities are made of 6061 aluminum alloy, in three different shapes, including two-dimensional cavity (cylinder) and three-dimensional cavities (hemisphere, truncated cone). The heights H-C of the cylindrical cavities are 1, 2, and 3 mm, respectively. The diameters D-C are 4, 5, and 6 mm, respectively. The height of the truncated cone cavity H-T is 2, 3 mm; the lower bottom diameter d is 2 mm, and the upper bottom diameter D-T is 4, 5, and 6 mm, respectively. The hemispherical cavity has a diameter of 2 mm in laser incidence direction, cavity height H–T is 3 mm, hemispherical diameter D–H is 4, 5, and 6 mm, respectively. The height of the cavity H–T is 2 mm, and the diameter is 4 mm.

2.2 Sample preparation

The medium-sized pig feed purchased from the market is pulverized using a grinder (400Y, Platinum Hardware factory) and sieved using a 60-mesh screen (sieved to <0.42 mm). Then, the nano-scale zinc oxide powder (≥99.9% purity) is added. This mixture is juddered at a constant speed by using a VORTEX 6 oscillator to obtain a uniform mixture. Using an automatic tablet press, 3 g samples are pressed into round cakes having a diameter of 25 mm and a thickness of 3 mm for performing tests. There are seven groups of samples with three pieces in each group. The reference concentration of Zn in pig feed samples was determined according to the method in GB/T 13885-2017, and the reference concentration obtained after three average measurements for each sample was listed in Table 1

2.3 Experimental method

In order to improve the stability of the LIBS signal and the repeatability of the experiments, optimized double pulse A energy is set at 195.5 mJ and B energy is set at 216.6 mJ. The time interval between two pulses is 0.9 μs, and the delay is 1.28, 1.58, 1.78, 1.88, 2.08, and 2.38 μs. The LIBS

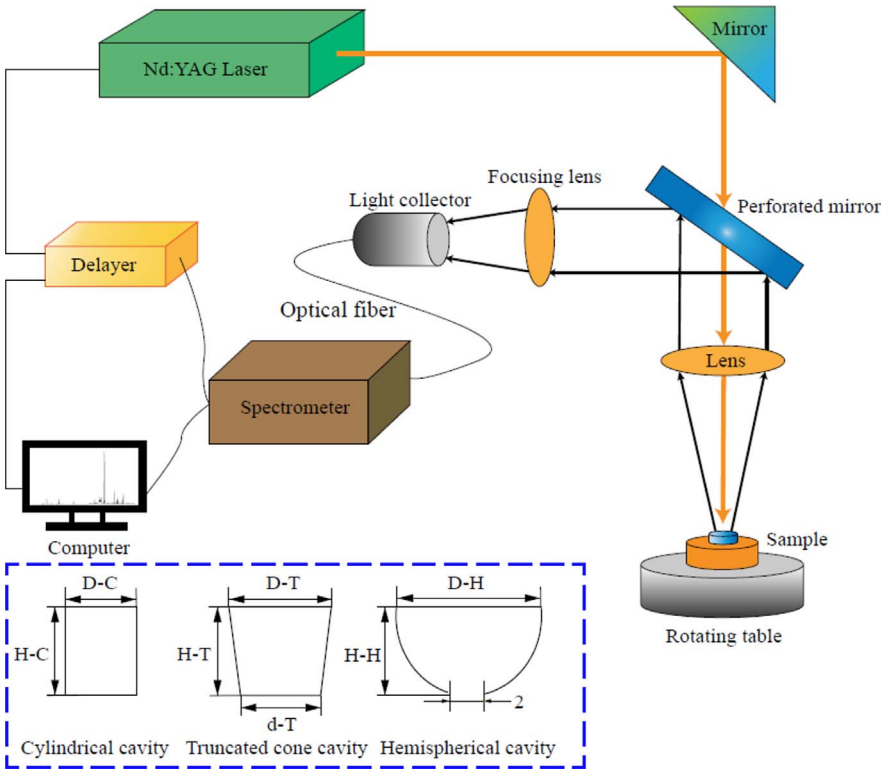

Figure 1. A schematic diagram of the experimental setup used in this work.

Table 1. The actual content of zinc in the samples of pig feed (mg/kg).

Sample	Reference concentration
1#	260.605
2#	314.6
3#	336.41
4#	340.165
5#	433.045
6#	434.435
7#	476.61

spectrum of samples is collected under both the traditional LIBS and CC-LIBS systems. The data of 50 different points of laser ablations on the surface of each sample are collected. Afterwards, the spectral map of the sample is obtained by calculating the average value. Three parallel samples are collected with different element concentrations.

According to the standard atomic spectrum database put forward by the National Institute of Standards and Technology and the characteristic wavelengths collected during the experiments, the main characteristic spectral lines of zinc element in this study include Zn I 467.83 nm, Zn I 472.03 nm, and Zn I 480.86 nm. Figure 2 shows the LIBS spectra of 7# samples in the band range of 466.9 nm – 481.7 nm. It is evident that the LIBS system effectively detects the spectral signal of zinc. As the spectral line intensity of Zn I 480.86 nm is higher, it is selected as the analytical spectral line in this work.

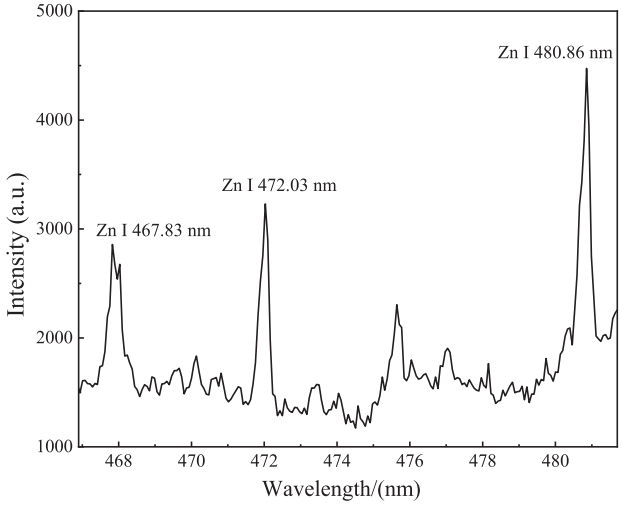

Figure 2. The LIBS spectra of 7# sample in the band of 466.9 nm–481.7 nm.

3 Results and discussion

3.1 Influence of cylindrical cavity on the enhancement factor

When the delay time are 1.28, 1.58, 1.78, 1.88, 2.08, and 2.38 μs, the enhancement factor of cylindrical cavities with different diameters and heights on the characteristic spectral lines is presented in Figure 3. It is evident that the enhancement factor fluctuates within a certain range.

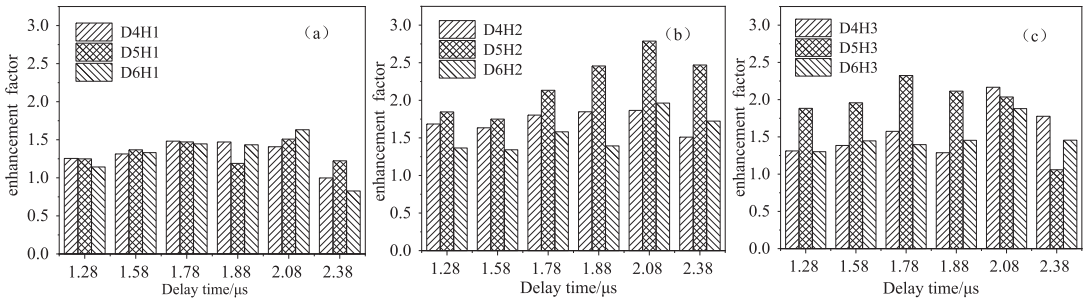

Figure 3. The effect of different cylindrical cavities on the enhancement factor with delay time. (a) cylindrical cavities of different diameters with a height of 1 mm, (b) cylindrical cavities of different diameters with a height of 2 mm, and (c) cylindrical cavities of different diameters with a height of 3 mm.

Figure 3 also shows that the sizes of different cylindrical cavities change with delay time, and the enhancement factor depicts two trends. First, the enhancement effect initially increases and then decreases with delay time. This is because the shock wave is uniformly reflected after it encounters the cavity during the process of diffusion and propagates back towards the center of the plasma, thus compressing the plasma and enhancing the spectral line maximally. Afterwards, the shock wave no longer interacts with the plasma, and the plasma begins to diffuse outwards and the intensity of spectral line gradually declines, resulting in a decrease in the enhancement factor. Second, the enhancement factor initially increases and then decreases with delay time, and then increases and decreases again. After the shock wave compresses the plasma, the plasma edge dissipates gradually. At this time, the confined cavity still enhances the plasma, and the enhancement effect gradually decreases due to the dissipation of the outer edge of plasma. However, when the plasma edge diminishes, the shock wave interacts directly with the plasma core, thus increasing the enhancement effect again, until the plasma also disintegrates gradually, and the enhancement effect again starts decreasing slowly. Regardless of the enhancement curve, the peak of the enhancement factor only appears at the delay time of 1.78 or 2.08 μs, indicating that the shock wave compresses part of the plasma at delay time of 1.78 μs and compresses the plasma core at delay time of 2.08 μs.

It is observed that the enhancement factor first increases and then decreases with an increase in the diameter of the cavity. This is because when the diameter of cavity is 4 mm, a certain part of the plasma and the cavity wall directly contact and dissipate, and the rest of the plasma is compressed by shock wave reflection. Consequently, the enhancement effect is not very obvious. When the diameter increases to 5 mm, the shock wave separates from the plasma, resulting in more compressed plasma, and a maximum enhancement factor is achieved. When the diameter increases to 6 mm, the distance of the shock wave before reflection increases, and the restraint effect of the cavity on it weakens. As a result, the enhancement effect decreases. Similarly, a cavity height of 1 mm causes the wall of the cavity to compress only part of the plasma. When the height of the cavity increases to 2 mm, the amount of compressed plasma increases, which in turn increases the enhancement factor. Furthermore, when the height of the confined cavity increases to 3 mm, part of the plasma annihilates in the cavity and the spectrometer is unable to acquire it. Thus, the enhancement effect reduces.

When the diameter and depth of a confined cavity are different, the spectral intensity obtained is also different. This shows that the cavity size plays a crucial role in the intensities of spectral lines. The results show that the maximum enhancement factor corresponds to cylinder D5H2, an enhancement factor of 2.79 at delay time 2.08 μs.

3.2 Influence of truncated cone and hemispherical constraint on the enhancement factor

The enhancement factors associated with characteristic spectral line intensities with varying delays time are illustrated in Figure 4 for differently sized truncated cone and hemispherical cavities. The enhancement trends of truncated cones and hemispherical cavities are similar to the aforementioned cylindrical cavities. Comparing the truncated cone cavities with different big ends diameters, heights and the hemispherical cavities with different diameters of presented in Figure 4, it is evident that the optimal enhancement factor is 3.01. The corresponding cavity shape is a truncated cone cavity (D5H3), and delay time is 2.08 μs. Here, it makes more sense to enhance the characteristic spectral lines as compared to the aforementioned constrained two-dimensional cavity. Since the plasma is assumed to be isotropic in the radial direction centered on the laser beam, as compared with the enhancement effect of the two-dimensional cylindrical cavity, the compression effect of the three-dimensional truncated cone cavity on the plasma only exists in a certain direction and is three-dimensional. Therefore, this optimal parameter is used for performing subsequent quantitative analysis.

3.3 Quantitative analysis with univariate calibration

The univariate method is based on the quantitative analysis of the relationship between the concentration of the target element and the emission spectral intensity of a standard sample. It uses LIBS and CC-LIBS calibration curves, as presented in Figure 5.

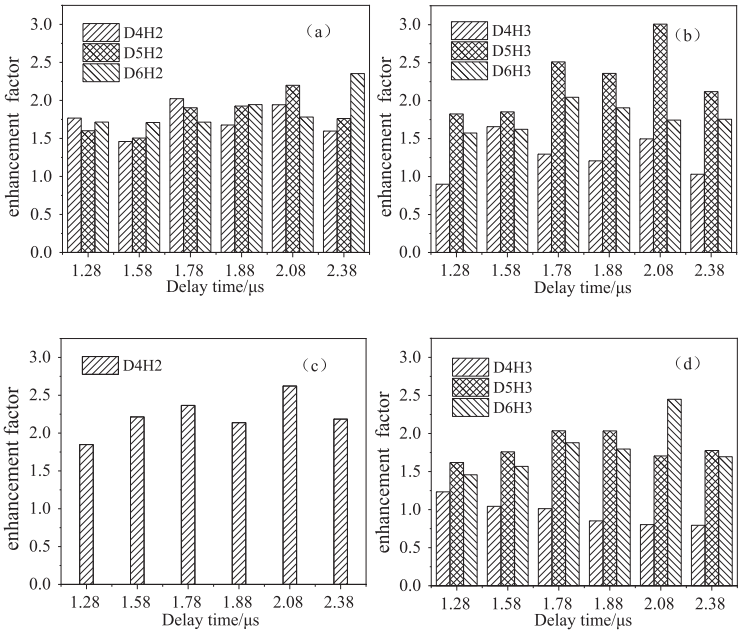

Figure 4. The effect of truncated cone and hemispherical cavities on the enhancement factor with delay time, (a) truncated cone cavities of different diameters of 2 mm height, (b) truncated cone cavities of different diameters of 3 mm height, (c) hemispherical restraint with a height of 2 mm and a diameter of 4 mm, and (d) hemispherical cavities of different diameters with a height of 1 mm.

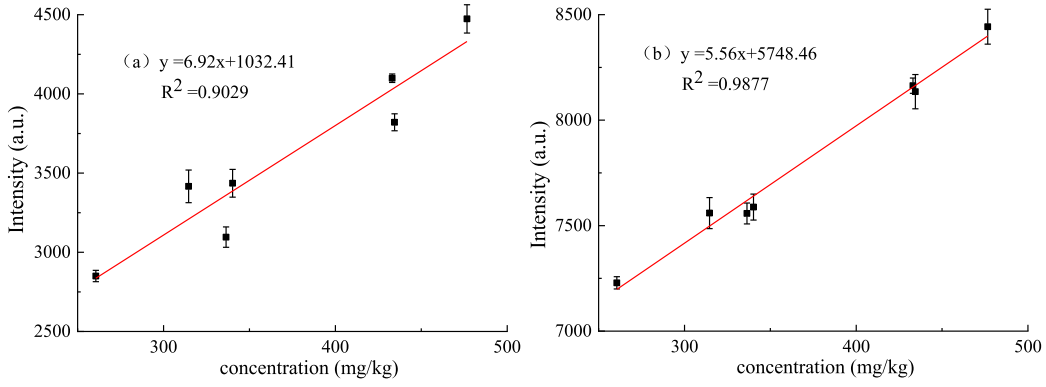

Figure 5. A single variable calibration curve. (a) LIBS and (b) CC-LIBS.

In order to study the detection sensitivity of CC-LIBS towards zinc present in pig feed, the element detection limit is roughly estimated using the following expression:

$$\mathrm{LOD} = 3\sigma/S, \tag{1}$$

where, σ denotes the background standard deviation and S denotes the linear slope of the calibration curve. The calculation results show that CC-LIBS not only improves the prediction accuracy of the model, but increases R^2 from 0.9029 to 0.9877 and reduces the detection limit from 97.39 mg/kg to 62.67 mg/kg. The CC-LIBS is 35.65% lower than the detection limit under LIBS. According to the Announcement No. 2625 by the Ministry of Agriculture of the People's Republic of China, the recommended dietary content of zinc in the feed produced for pigs is 43–80 mg/kg, as presented in the code for the safe use of feed addition. Therefore, CC-LIBS successfully detects the pig feed samples containing excessive quantities of zinc.

The CC-LIBS system presented in this work significantly reduces the detection limit of zinc in the LIBS system. Therefore, the proposed method has a potential application value in the rapid and sensitive analysis of zinc in pig feed samples.

4 Conclusions

In order to study the radiation enhancement effect of the confined cavity on laser-induced plasma, in this work, cylindrical, hemispherical, and truncated cone cavities of different sizes are used to spatially constrain the plasma generated by laser ablation of pig feed. The atomic spectral line of Zn I 480.86 nm in the plasma radiation is selected as

the analytical spectral line. The optimum enhancement factor of the spectral line intensities under different delays time, and for different shapes and sizes of constrained cavities are analyzed. The experimental results presented in this work show that the truncated cone cavity D5H3 is the optimal cavity. The delay time corresponding to the best enhancement ratio is 2.08 μs. The best enhancement ratio to the analytical spectral line is 3.01. The detection limit of zinc under the proposed CC-LIBS is 35.65% lower as compared to the LIBS system, which meets the requirements put forward by the national detection standards. The results make it evident that the cavity confined LIBS not only increases the spectral intensity, but it also improves the sensitivity of LIBS and reduces the detection limit.

Conflict of interest

The authors declare no conflict of interest.

Acknowledgments. This work is supported by National Natural Science Foundation of China (NSFC) Grant No. 31960363.

References

1 LaRosae M.N., Samuel R.S., Clizer D.A. (2022) 116 effect of zinc oxide and organic zinc on weanling pig performance, *J. Animal Sci.* **100**, Suppl 2, 52.
2 National Research Council, Division on Earth and Life Studies, Board on Agriculture and Natural Resources, Committee on Nutrient Requirements of Swine (2012) *Nutrient requirements of swine*, National Academies Press.
3 Bonetti A., Tugnoli B., Piva A., Grilli E. (2021) Towards zero zinc oxide: feeding strategies to manage post-weaning diarrhea in piglets, *Animals* **11**, 3, 642.
4 Hansen S.V., Nørgaard J.V., Woyengo T., Nielsen T.S. (2023) The relationship between zinc intake, dietary content, and fecal excretion in pigs, *Livest. Sci.* **271**, 105228.
5 Tella M., Legros S., Monteiro A.N.T.R., Forouzandeh A., Penen F., Durosoy S., Doelsch E. (2023) Unexpected Cu and Zn speciation patterns in the broiler feed-animal-excreta system revealed by XAS spectroscopy, *Chemosphere* **340**, 139684.
6 Monteiro S.C., Lofts S., Boxall A.B. (2010) Pre-assessment of environmental impact of zinc and copper used in animal nutrition, *EFSA Support. Publ.* **7**, 9, 74E.
7 Poole K. (2017) At the nexus of antibiotics and metals: the impact of Cu and Zn on antibiotic activity and resistance, *Trends Microbiol.* **25**, 10, 820–832.
8 Announcement No. 2625 (2018) Ministry of Agriculture of the People's Republic of China, *Hunan Feed* **01**, 17.
9 Lusha S., Zhicun G., Hunjan C., Shuning Y., Yun G. (2022) Evaluation of uncertainty for determination of zinc content in feed by atomic absorption spectrometry, *China Metrol.* **05**, 99–101.
10 Ya M. (2019) Spectrophotometric determination of zinc in animal feed, *Guangdong Chem. Indus.* **46**, 09, 223–224.
11 Jianli H., Huang L., Lingfeng C. (2019) Determination of Na, Mg, Cr, Mn, Fe, Cu, Zn, As, Se, Cd and Pb in animal feed by ICP-MS, *Feed Indus.* **40**, 18, 54–58.
12 Darshitsinh P., Rohit S.K.B.P. (2023) Laser induced breakdown spectroscopy: A robust technique for the detection of trace metals in water, *Mater. Today Proc.* 77, P1.
13 Cui M., Guo H., Chi Y., Tan L., Yao C., Zhang D., Deguchi Y. (2022) Quantitative analysis of trace carbon in steel samples using collinear long-short double-pulse laser-induced breakdown spectroscopy, *Spectrochim. Acta B* **191**, 106398.
14 Wang Q., Chen A., Chen Y., Jiang Y., Liab S., Jin M. (2021) Highly sensitive analysis of trace Pb in aqueous solution using electro-deposition and spark-discharge assisted laser-induced breakdown spectroscopy, *J. Anal. At. Spectrom.* **36**, 1889–1894.
15 Awan R.A., Siraj K., Haq S.U., Abbas Q., Rahim M.S.A., Younas Q., Fareed S., Ahsen R., Ahmad Z., Irshad M., Latif A. (2023) Laser induced breakdown spectroscopy of aluminum incorporated with metallic nanoparticles, *Opt. Quantum Electron.* **55**, 1, 73.
16 Ikeda Y., Soriano J.K., Ohba H., Wakaida I. (2023) Analysis of gadolinium oxide using microwave-enhanced fiber-coupled micro-laser-induced breakdown spectroscopy, *Sci. Rep.* **13**, 1, 4828.
17 Hussain A., Iqbal S.T., Shahbaz R.M., Zafar M., Arshad A. A., Aslam K., Mukhtar M. (2022) Varying magnetic field strength as an effective approach to boost up the plasma signal in laser-induced breakdown spectroscopy, *Heliyon* **8**, 9.
18 Fu Y., Hou Z., Wang Z. (2016) Physical insights of cavity confinement enhancing effect in laser-induced breakdown spectroscopy, *Opt. Exp.* **24**, 3, 3055–3066.
19 Xue Y., Anmin C., Suyu L., Jiang Y., Mingxing J. (2020) Effect of parallel plate constraint on CN molecular Spectra in laser-induced PMMA plasma, *Chin. J. Lasers* **47**, 08, 271–277.
20 Chen J.Z., Ma R.L., Wang J., Li X., Su H.X. (2014) Study of self-absorption effect on laser-induced metal plasma, *Spectrosc. Spec. Anal.* **34**, 09, 2337–2341.
21 Wang Y., Jia Y., Gao L., Su Q., Liu W., Zhou T., Xiao Q. (2023) The effects of cavity diameter and material type of spatial confinement on intensity of laser-induced breakdown spectroscopy, *Phys. Scr.* **98**, 1, 015610.
22 Xu B., Liu Y., Lei B., Wang J., Zhang W., Wang Y., Zhao W., Duan Y., Tang J. (2022) Comparative study on the copper plasma confined with upward and downward conical cavities in laser-induced breakdown spectroscopy, *Spectrochim. Acta B* **197**, 106528.
23 Meng D., Zhao N., Ma M., Wang Y., Hu L., Yu Y., Fang L., Liu W. (2015) Heavy metal detection in soils by laser induced breakdown spectroscopy using hemispherical spatial confinement, *Plasma Sci. Technol.* **17**, 8, 632.
24 Li A., Guo S., Wazir N., Chai K., Liang L., Zhang M., Hao Y., Nan P., Liu R. (2017) Accuracy enhancement of laser induced breakdown spectra using permittivity and size optimized plasma confinement rings, *Opt. Exp.* **25**, 22, 27559–27569.
25 Meng Y., Li H., Wang Y., Lv H., Wang C., Wang F., Fang L. (2023) Influence of planar mirror confinement and temperature control upon the elemental analysis of soil by laser-induced breakdown spectroscopy, *Anal. Lett.* **56**, 17.
26 Ren L., Hao X.-J., Yang Y.-W., Sun Y.-K. (2020) Time evolution characteristics of laser-induced breakdown spectroscopy under combined action of cavity confinement and nanoparticles, *Spectrosc. Spect. Anal.* **40**, 4, 1012–1017.